ELSEVIER

Fluid Phase Equilibria 183–184 (2001) 351–361

FLUID PHASE EQUILIBRIA

www.elsevier.com/locate/fluid

Transport properties of fluids: symplectic integrators and their usefulness

J. Ratanapisit [a,b], D.J. Isbister [c], J.F. Ely [b,*]

[a] *Chemical Engineering and Petroleum Refining Department, Colorado School of Mines, Golden, CO 80401, USA*
[b] *Department of Chemical Engineering, Prince of Songla University, Hat-Yai, Songkla 90110, Thailand*
[c] *School of Physics, University College, University of New South Wales, ADFA, Canberra, ACT 2600, Australia*

Abstract

An investigation has been carried out into the effectiveness of using symplectic/operator splitting generated algorithms for the evaluation of transport coefficients in Lennard–Jones fluids. Equilibrium molecular dynamics is used to revisit the Green–Kubo calculation of these transport coefficients through integration of the appropriate correlation functions. In particular, an extensive series of equilibrium molecular dynamic simulations have been performed to investigate the accuracy, stability and efficiency of second-order explicit symplectic integrators: position Verlet, velocity Verlet, and the McLauchlan–Atela algorithms. Comparisons are made to nonsymplectic integrators that include the fourth-order Runge–Kutta and fourth-order Gear predictor–corrector methods. These comparisons were performed based on several transport properties of Lennard–Jones fluids: self-diffusion, shear viscosity and thermal conductivity. Because transport properties involve long time simulations to obtain accurate evaluations of their numerical values, they provide an excellent basis to study the accuracy and stability of the SI methods. To our knowledge, previous studies on the SIs have only looked at the thermodynamic energy using a simple model fluid. This study presents realistic, but perhaps the simplest simulations possible to test the effect of the integrators on the three main transport properties. Our results suggest that if an algorithm fails to adequately conserve energy, it will also show significant uncertainties in transport property calculations.

Keywords: Gear predictor–corrector; Lennard–Jones fluid; McLauchlan–Atela; Molecular dynamics; Position Verlet; Self-diffusion coefficient; Shear viscosity; Thermal conductivity; Symplectic integrators; Velocity Verlet

1. Introduction

The characterization of transport properties of liquids has significantly benefited from numerical simulation techniques. In particular, both equilibrium (EMD) and nonequilibrium molecular dynamics (NEMD) have provided valuable data that can be used to test and extend transport theories for systems of known

* Corresponding author.
E-mail address: jely@mines.edu (J.F. Ely).

0378-3812/01/$20.00
PII: S0378-3812(01)00447-2

intermolecular potentials [1–4]. The diffusion, viscosity and thermal conductivity coefficients were originally studied by equilibrium MD simulations via the Green–Kubo linear response theory. Verlet [5–7] and Rahman [8] independently performed simulations of a Lennard–Jones liquid for its equilibrium and transport properties, respectively. Hoover et al. [9] extended the Green–Kubo (GK) technique for viscosity via a more demanding integration of the stress correlation function. A corresponding equilibrium simulation of the thermal conductivity of Lennard–Jones fluids was performed by Hoheisel and Vogelsang [10]. These equilibrium simulations illustrated system size dependence properties, cancellation of positive and negative areas under the time integral of the correlation function being calculated and treated the linear response of the system to some appropriate driving term. However, in these studies, relatively short time runs ($\sim$5 ps) were used to calculate transport and equilibrium properties to an estimated accuracy of $\pm 5\%$.

Nonequilibrium MD techniques were pioneered by Hoover [2,3] and Evans [11] in common applications to shear viscosity. Evans and coworkers also introduced NEMD techniques to evaluate the thermal conductivity. In the area of diffusion, Holian [9] used NEMD to calculate the color diffusion of a binary mixture of Lennard–Jones particles and then extrapolated the inter-color diffusion to a color-independent value. Later, this method was modified by Evans into what is now known as the color diffusion algorithm. Unlike the earlier simulation, Evans introduced a hot and cold colored particle scheme in which the color variable was simply coupled to the external color field $c_i = \pm 1$. A synthetic Hamiltonian was constructed so as to reproduce the linear response theory limit as the field strength approached zero.

Several authors have compared the two different methods for transport property simulation. Schoen and Hoheisel [12] used the Green–Kubo relation to calculate the shear viscosity at various conditions by MD simulations for a LJ fluid, employing the Stormer–Verlet integration scheme. The computations were performed for 32–2048 particles. Overall, the results showed about 30% difference from Levesque's MD yet were in good agreement with the NEMD results obtained by Heyes [13–15]. A significant number dependence was found for particle numbers less than 256 [12]. In 1988, Hoheisel and Vogelsang [10] determined transport coefficients of pure liquids and binary mixtures by both nonequilibrium (NEMD) and equilibrium (EMD) molecular dynamics. Satisfactory agreement with experimental diffusion and shear viscosity data was found (to within their stated errors). For the bulk viscosity, they found the MD values 10% smaller than the experimental bulk viscosities which carry relatively large (20–30%) errors. Erpenbeck [16] performed Green–Kubo calculations and conclusively showed that the stress autocorrelation exhibited a slow decay mainly due to a large potential contribution.

The diffusion constants obtained from both equilibrium and nonequilibrium approaches are in excellent agreement. In general, nonequilibrium MD simulations seem to suppress the system size dependence (N-dependence) of simulated properties and physically identify the flux (color, stress tensor, heat flux) per unit field (color field, strain rate, heat field) as color conductivity (closely related to the diffusion constant), viscosity and thermal conductivity. Despite the unexpectedly small N-dependence of this type of simulation, relatively long time runs are required to ensure the system achieves a nonequilibrium steady-state. Effectively the longer runs required by the NEMD simulations included corrections to the time truncation of the correlation functions often found in the equilibrium simulations. An excellent review of the history behind the early NEMD works can be found in separate texts by Hoover [2,3] and Evans and Morriss [4].

Recently, numerous simulation studies have centered on the stability and energy conserving properties of symplectic numerical integrators. These integrators were well known to high energy physicists and astronomers since the early sixties, but have only been recently discovered in liquid state theory applications. Discussion of some of the early developments in this area can be found in [17–19]. The

liquid state community was initiated to these symplectic methods by Berne and Tuckermann [20–22] as well as independently by Yoshida [18,19]. It is interesting to note that the pioneering works of Verlet and Rahman can be contrasted nowadays in the use of symplectic and nonsymplectic (specifically the traditional Runge–Kutta) algorithms respectively. Many of the later applications have concentrated on the energy conserving property of these symplectic integrators for systems ranging from simple spherical interactions to sophisticated polymer models with both short and longer ranged forces. Xu [23] studied viscosity in polymer solutions; Stevens et al. [24] modeled polymer flow in butane-lined channels for thermostatted conditions; Tuckermann et al. [25,26] studied the quantum mechanical simulations of the Car-Parinello problem using appropriate symplectic integration.

In this paper, we revisit the original calculations of the diffusion, viscosity and thermal conductivity coefficients using the Green–Kubo formalism in which the equations of motion are solved with symplectic integration schemes. Our motivation for reevaluation of the classical Green–Kubo approach lies in the belief that the time averaging of many trajectories in the appropriate time correlation function might counter the accuracy of the symplectic integration routines. It is not obvious that the enriched areas of phase space opened up by symplectic integration significantly contribute to the transport coefficients. In Section 2, we summarize the Green–Kubo formalism for the transport properties under study and in Section 3, we discuss the simulation details. Our results and conclusions are given in Section 4.

2. Theory

It is well established that linear response theory gives the fluctuation–dissipation formula for the diffusion constant D as the time integral of the velocity autocorrelation function as

$$D = \frac{1}{3}\int_0^\infty \mathrm{d}t\,\langle \boldsymbol{v}(0)\boldsymbol{v}(t)\rangle \tag{1}$$

D can be equivalently defined by the Einstein formula as the long time gradient of the mean square displacement vector

$$D = \lim_{t\to\infty} \frac{\langle(\boldsymbol{r}(t) - \boldsymbol{r}(0))^2\rangle}{6t} \tag{2}$$

Similarly the viscosity η for planar flow is the time integral of the stress autocorrelation function

$$\eta = \frac{V}{kT}\int_0^\infty \mathrm{d}t\,\langle P_{xy}(0)\,P_{xy}(t)\rangle \tag{3}$$

where P_{xy} is the xy-component of the pressure tensor P given as

$$\boldsymbol{P} = \sum_{i=1}^{N} \frac{\boldsymbol{p}_i\boldsymbol{p}_i}{m} - \frac{1}{2}\sum_{1\le i,j\le N} \boldsymbol{r}_{ij}\boldsymbol{F}_{ij} \tag{4}$$

Integration of Eq. (3) gives rise to three contributions to the viscosity-the kinetic (involving only the momentum terms from Eq. (4)), cross and potential (involving only the force and position terms from Eq. (4)).

The thermal conductivity λ is associated with the heat flux correlation function

$$\lambda = \frac{V}{kT^2}\int_0^\infty \mathrm{d}t\,\langle \boldsymbol{J}_q^x(t)\boldsymbol{J}_q^x(0)\rangle \tag{5}$$

with

$$\boldsymbol{J}_q = \frac{m}{2}\sum_{i=1}^{N}\boldsymbol{v}_i^2\boldsymbol{v}_i - \frac{1}{2}\sum_{i\neq j}[r_{ij}\nabla u(r_{ij}) - u(r_{ij})\boldsymbol{I}]\boldsymbol{v}_i \tag{6}$$

Here $\boldsymbol{r}_{ij} = \boldsymbol{r}_j - \boldsymbol{r}_i$ is the interparticle distance vector from particle i to j and $\boldsymbol{F}_{ij} = -\nabla u(r_{ij})$ is the force being exerted on particle i by particle j. In all of these equations, the angular brackets $\langle\,\rangle$ indicate an ensemble average over an equilibrium distribution $f(\Gamma)$ of the phase variables Γ.

3. Simulation details

The MD simulations were carried out on a system of 256 Lennard–Jones particles at the triple point, where the reduced temperature and density are $T^* = kT/\varepsilon = 0.722$ and $\rho^* = \rho\sigma^3 = 0.8442$, respectively. A series of simulations were run, each starting from the same initial configuration, with each simulation being run the same reduced time, namely $t^* = 1000$. The reduced time-steps considered are: $\Delta t^* = \Delta t\,(m\sigma^2/\varepsilon)^{1/2} = 0.0025, 0.005, 0.010, 0.015, 0.020$. The Lennard–Jones potential is defined as usual

$$u(r) = \begin{cases} 4\varepsilon\left(\left(\dfrac{\sigma}{r}\right)^{12} - \left(\dfrac{\sigma}{r}\right)^{6}\right) & \text{if } r \le r_{\mathrm{cut}} \\ 0 & \text{otherwise} \end{cases} \tag{7}$$

where the cut-off radius was taken as $r_{\mathrm{cut}} = 2.5\sigma$. A selection of numerical integrators was tested including traditional algorithms (usually nonsymplectic) and the more recent symplectic integrators (SI). For historical reasons, we chose the fourth-order nonsymplectic Gear (G4) and Runge–Kutta (RK4) [27], as well as the second-order, time-invertable symplectic [20–22] position-Verlet (pV2) and velocity-Verlet (vV2) and a noninvertable second-order algorithm optimized by McLachlan and Atela (MA2) [28]. The three symplectic algorithms investigated in this study are summarized in Table 1.

The simulation runs were divided into 10 independent batches such that these 10 batches formed an approximate Gaussian distribution for which the mean and its uncertainty can be calculated. This block sampling technique gives reliable error estimates from computer simulations.

Table 1
Summary of nonpredictor–corrector algorithms[a] investigated

Integrators	Order	Force evaluations	Coefficients
Ruth [17], position Verlet [21]	2	1	$a_1 = 1/2, a_2 = 1/2, b_1 = 0, b_2 = 1$
Velocity Verlet [21]	2	1	$a_1 = 0, a_2 = 1, b_1 = 1/2, b_2 = 1/2$
McLachlan and Atela [28]	2	2	$a_1 = 1/\sqrt{2}, a_2 = 1 - a_1, b_1 = 1/\sqrt{2}, b_2 = 1 - b_1$

[a] Basic algorithm pseudo-code: for $(k = 1, 2)\{\boldsymbol{p}^{(k)} = \boldsymbol{p}^{(k-1)} + b_k\Delta t\boldsymbol{F}(\boldsymbol{q}^{(k-1)});\ \boldsymbol{q}^{(k)} = q^{(k-1)} + a_k\Delta t G(p^{(k)})\}$, where $\boldsymbol{F}$ is the force and G the Hamiltonian derivative with respect to momentum.

4. Results and discussion

4.1. Energy conservation

Energy conservation provides useful information to study the characteristic of SIs and has been the basis for most SI evaluations presented in the literature. For NVE (e.g. unconstrained Hamiltonian-based simulations), the expectation value of the energy should be constant. In fact, the degree to which the energy is conserved is often used to monitor the efficacy of various parts of the simulations. Energy conservation results for the integrators used in this study are summarized in Table 2 which compares the average total energy drift $\langle H(t)\rangle - H(0)$ as a function of reduced time-step size and integration method. Each algorithm was employed to generate the energy out to a common reduced time of $t^* = 1000$. As expected, the nonSIs (RK4 and G4) show significant deviations from the initial total energy. Also, G4 becomes unstable well before the other four algorithms. G4 is stable at a reduced time-step of 0.001, but begins to exhibit significant deviations at a time-step of 0.0025. The energy deviations observed for G4 can be improved by rescaling the velocity every 5000 time-steps with the net result that the method then allows simulation runs up to a time-step of 0.005. For time-steps larger than 0.005, the G4 simulations become unstable, both with and without velocity scaling.

In general, instabilities in these algorithms reflect the discrete nature of the numerical solution of the equations of motion. If the time-step size is too large, the displacement during one time-step results in an erroneous particle overlap, which does not occur if particles experience continuous change in their interaction potential. If two particles find themselves severely embedded in their repulsive cores after a large time-step, steep repulsive LJ potential causes a very large repulsive force between the pair. This causes an enormous change in the pair's dynamics and causes them to fly apart at huge velocities. Evidence of too long of a time-step can be found in: large fluctuations of the total energy of the system; a very large rise in the velocity of some of the particles; or the simulation "melting down" with a very large temperature.

Although the second-order MA is not time-reversible, it is very competitive or even better than the Verlet methods in the limit of large time-steps. This is probably due to the fact that the MA algorithm was derived on the basis of the Ruth SI, except that the coefficients were chosen to minimize the error associated with the Δt^2 term. Its numerical scheme shows a connection between the decomposition process such that at each step the evolution of the system under the Hamiltonian contains the solution involving the potential contribution for a time $b_k \Delta t$ followed by the consideration of the kinetic contribution for a time $a_k \Delta t$. These schemes are different than G4 in that the force prediction in G4 is irrelevant to the correction process

Table 2
Calculated total energy drift $\langle H(t)\rangle - H(0)$ obtained for various numerical algorithms and time-step-sizes

Method	Reduced time-step				
	0.0025	0.005	0.010	0.015	0.020
pV2	0.0004249	0.0009577	0.0035131	0.0047460	0.0394091
vV2	0.0001994	0.0013480	0.0023139	0.0037985	0.0744680
MA2	0.0001551	0.0007414	0.0021894	0.0034915	0.0332518
G4	0.0038772	–	Overflow	Overflow	Overflow
RK4	−0.0015252	−0.0467584	−0.4709937	−0.9894928	−2.587943

for the position. All results indicate that the SI methods not only are better than the nonSIs during the long time simulations, but also allow larger time-steps to be used with acceptable uncertainties. Results for energy conservation suggest that the position Verlet is better in the limit of large time-steps, whereas the velocity Verlet is better in the limit of small time-steps. These results support the conclusions of Tuckerman [21].

4.2. Diffusion coefficients

Diffusion coefficients in this work were calculated from both the mean square displacement (the Einstein expression) and the Green–Kubo expressions given above. Table 3 summarizes the diffusion and viscosity simulation results. Satisfactory agreement of the diffusion coefficients was obtained with previous studies [8,10,16,29] with the generally accepted reduced value being 0.029 [30]. Fig. 1 displays the results obtained for the diffusion coefficients as a function of time-step-size using the Green–Kubo expression (open symbols) and MSD (solid symbols) relation Eq. (2). Even though, the diffusion coefficients in Table 3 were generated from the same initial configuration, the results from Einstein expression are consistently higher than those from the Green–Kubo expression. We note, however, that the precision of the Einstein extrapolated results tends to be less than those of the Green–Kubo calculations. Statistical analysis shows that the results from both expressions are not significantly different. Results at other

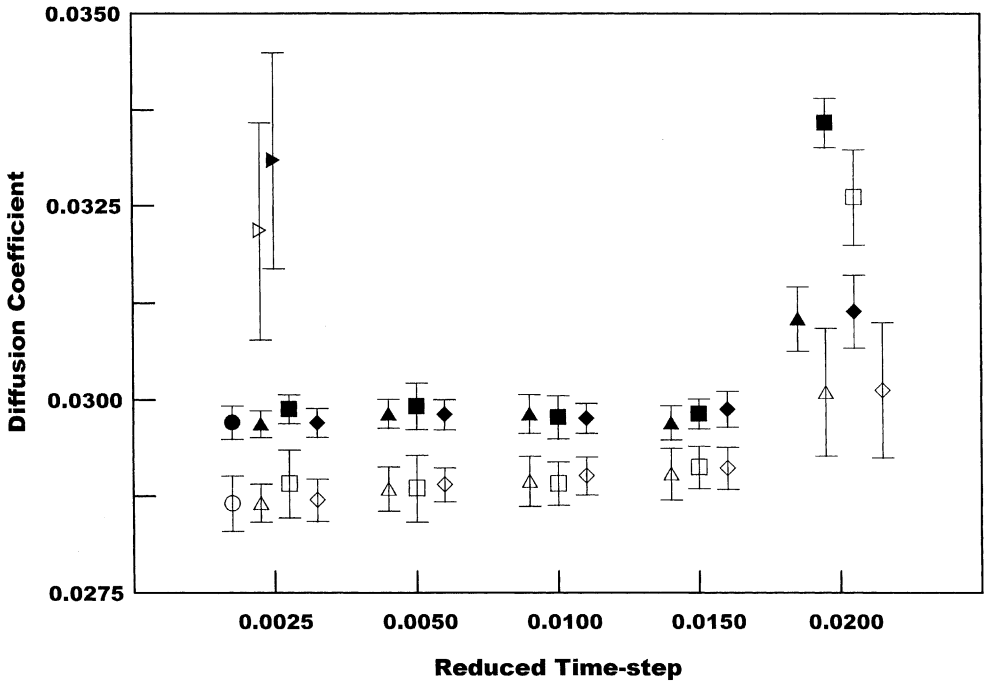

Fig. 1. Comparison of Green–Kubo diffusion coefficients as a function of time-step. The points have been offset around their time-step so that the error bars can be more clearly identified. Open symbols denote Green–Kubo results while solid symbols give the MSD results: (▷) G4; (○) RK4; (△) position Verlet; (□) velocity Verlet; (◇) McLachlan–Atela.

Table 3
Simulation results for diffusion coefficients and viscosity as a function of integration method and reduced time-step[a]

Property	Method	Time-step				
		0.0025	0.005	0.010	0.015	0.020
GK diffusion	pV2	0.028660 (0.000243)	0.028843 (0.000284)	0.028941 (0.000321)	0.029036 (0.000334)	0.030099 (0.000831)
	vV2	0.028908 (0.000337)	0.028848 (0.000332)	0.028912 (0.000279)	0.029121 (0.000274)	0.032612 (0.000618)
	MA2	0.028698 (0.000272)	0.028896 (0.000219)	0.029011 (0.000246)	0.029109 (0.000272)	0.030123 (0.000877)
	G4	0.032181 (0.001426)	0.030202 (0.000419)	Overflow	Overflow	Overflow
	RK4	0.028656 (0.000355)	0.026625 (0.001300)	0.020021 (0.001086)	0.021071 (0.001275)	0.010413 (0.001471)
MSD diffusion	pV2	0.029686 (0.000175)	0.029819 (0.000189)	0.029817 (0.000252)	0.029701 (0.000225)	0.031048 (0.000754)
	vV2	0.029880 (0.000190)	0.029914 (0.000302)	0.029772 (0.000281)	0.029819 (.000194)	0.033582 (0.000590)
	MA2	0.029702 (0.000187)	0.029808 (0.000199)	0.029760 (0.000196)	0.029878 (.000235)	0.031142 (0.000860)
	G4	0.033093 (0.001402)	0.030633 (0.000325)	Overflow	Overflow	Overflow
	RK4	0.029705 (0.000220)	0.027630 (0.001305)	0.021047 (0.001068)	0.020380 (0.001229)	0.012011 (0.001229)
Viscosity	pV2	3.1692 (0.2080)	3.2199 (0.2167)	3.2053 (0.2999)	3.1433 (0.3452)	3.2177 (0.3832)
	vV2	3.1751 (0.2901)	3.0833 (0.2643)	3.0731 (0.2915)	3.2351 (0.3743)	3.2075 (0.4589)
	MA2	3.0798 (0.2042)	3.3016 (0.2935)	3.2683 (0.3185)	3.1267 (0.2790)	3.4929 (0.3127)
	G4	3.4462 (0.3471)	3.4293 (0.3934)	Overflow	Overflow	Overflow
	RK4	3.04324 (0.2686)	3.3222 (0.3214)	2.8761[b] (0.2592)	2.9919[b] (0.3652)	3.3172[b] (0.5004)

[a] The first line is the average value and the second line represents its uncertainty, e.g. the first entry is 0.028660 ± 0.000243.
[b] Indicates momentum rescaling.

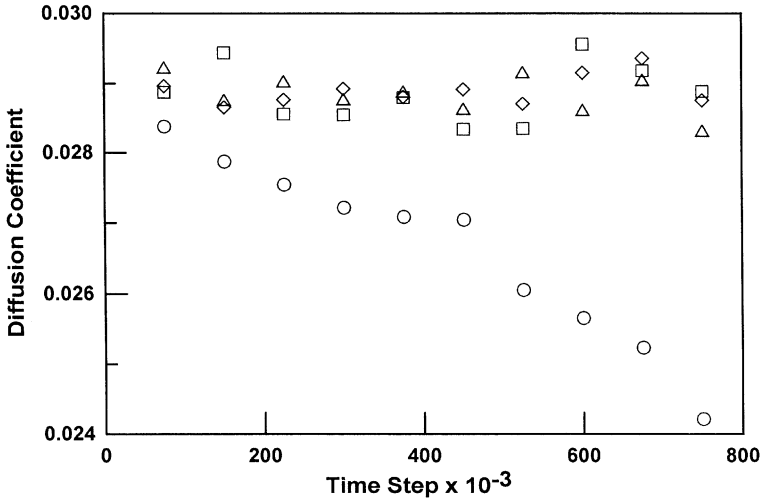

Fig. 2. Time evolution of the GK diffusion coefficient evaluated with a simulation time-step of $\Delta t^* = 0.005$: (○) RK4; (△) position Verlet; (□) velocity Verlet; (◇) McLachlan–Atela.

time-steps or other numerical methods for normalized autocorrelation functions essentially provide the same trend.

Even at a time-step $\Delta t^* = 0.005$, simulations based on G4 cannot generate reasonable results without using rescaling for momentum drift. For larger time-steps the G4 algorithm fails completely, even with velocity rescaling. As expected, the RK4 algorithm is more stable than the G4: for small time-steps it gives reasonable diffusion results without rescaling. However, deviations gradually appear for even a moderate time-step size. Fig. 2 shows the time dependence of the GK diffusion coefficient during a typical run at $\Delta t^* = 0.005$. The large time-step results for RK4 without rescaling show significant deviations and eventually become unphysical for $\Delta t^* > 0.01$. Fig. 1 clearly shows the advantages of the symplectic integrators, for large time-steps. All three algorithms provide physically acceptable results at large time-steps: more importantly they do so with uncertainties comparable to RK4 and G4 obtained using significantly smaller time-step sizes. It would be remiss of us not to point out that accurate diffusion constants can be generated (albeit expensively) from the RK4 algorithm for large time-steps by rescaling the velocities as often as possible. This constant updating significantly improves previous results as shown in Table 2.

For large time-steps, vV2 is less reliable than the pV2 and MA2 algorithms in agreement with Tuckerman's earlier [20] results for energy conservation. The diffusion results clearly show the time and precision advantages of symplectic integrators over nonsymplectic integrators with pV2 being considerably more reliable than all others at higher time-step size. Comparison between pV2 and vV2 methods suggests that pV2 may give slightly better results as seen in the uncertainties of the Einstein diffusion method. However, both algorithms are equally competitive for the GK results.

4.3. Shear viscosity

The shear viscosity provides a clearer picture of the advantages of SIs in long time simulations. Fig. 3(a) illustrates the results and uncertainties as a function of time-step and the numerical values obtained from

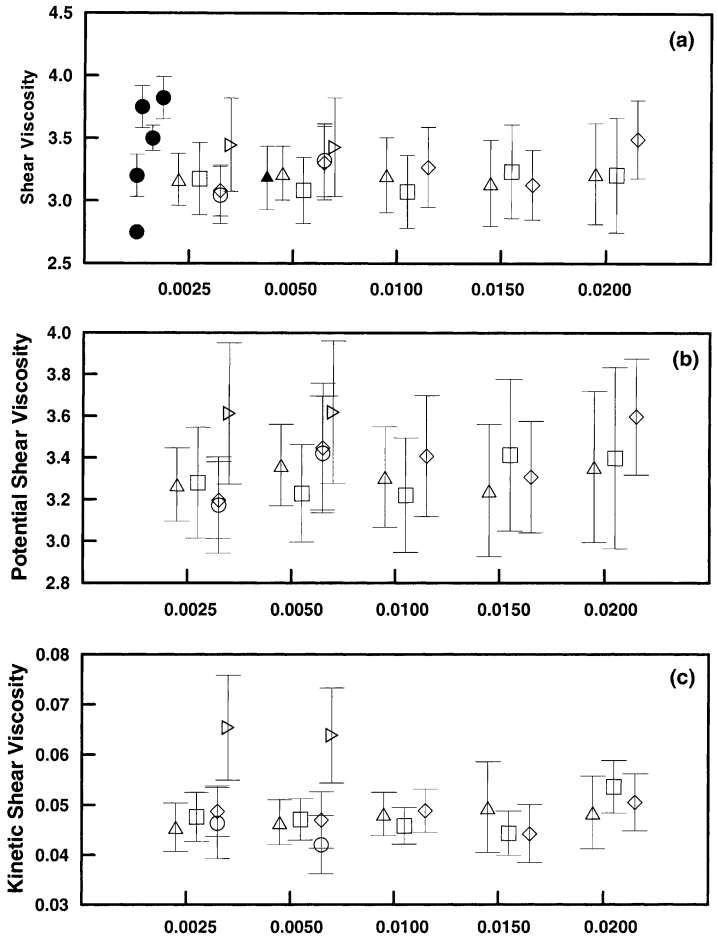

Fig. 3. Comparison of the overall shear viscosity (a), potential contribution to the viscosity (b) and kinetic contribution to the viscosity (c) as a function of time-step and integration method. The solid symbols are results reported by other investigators: (▷) G4; (○) RK4; (△) position Verlet; (□) velocity Verlet; (◇) McLachlan–Atela.

the GK expression (3) are presented in Table 3. Fig. 3(b) and (c), respectively show the calculated potential and kinetic contributions to the viscosity. In this work we found (on average) $\eta = 3.23$, whereas literature values were found to be 3.18 ± 0.26 by Hoheisel [10], 3.4 by Heyes [30], 3.77 ± 0.17 by Erpenbeck [16], and 2.72 by Levesque and Verlet [29]. The older value of Levesque is somewhat in question.

For small time-steps, uncertainties in the kinetic contribution to the viscosity obtained from vV2 are much smaller than pV2 while the latter provides a smaller error estimate for the potential contribution. The total shear viscosity from pV2 seems to be better than vV2, although their differences are not statistically significant. This is because the potential and cross-values and their errors dominate over the smaller kinetic contribution. For large time-steps, pV2 seems to provide more accurate and precise values for the both the kinetic and potential terms.

Further comparison between SI and nonSI methods reinforces the diffusion results and conclusions, but with much stronger evidence for the advantages of SI algorithms for shear viscosity simulations. RK4

Table 4
Thermal conductivity for different time-steps and algorithms

Method	Time-step				
	0.0025	0.005	0.010	0.015	0.020
pV2	6.8267 (0.5840)	6.8868 (0.6425)	6.6686 (0.6910)	6.7721 (0.7106)	6.9242 (0.8386)
vV2	6.8521 (0.4855)	6.8183 (0.6644)	6.8564 (0.5745)	6.8211 (0.7562)	6.9721 (0.8932)
MA2	6.8727 (0.5402)	6.8930 (0.6541)	6.7905 (0.6315)	6.9398 (0.7212)	6.9997 (0.8085)

gives very large uncertainties compared to the SI methods for both potential and kinetic contributions to the viscosity. For larger time-steps at which the SI methods converge, the nonSI algorithms are far too large and their results are not shown here.

Although not specifically reported in Table 3, the kinetic contribution to the shear viscosity obtained from RK4 is much less than those obtained from other algorithms. Also, a large deviation of the potential contribution from RK4 is found earliest among all algorithms and the associated shear viscosity is found to be greater than 100 with $\Delta t^* = 0.010$, a time-step for which the Verlet methods give a shear viscosity in the physically acceptable range of 3.0–3.3.

4.4. Thermal conductivity

The thermal conductivity is one of the most difficult transport coefficients to calculate [11] because of the long time relaxation of the heat flux vector when using the Green–Kubo approach. The typically accepted value for the reduced thermal conductivity is 6.9 [30]. Hoheisel and coworkers have previously used the Stormer–Verlet algorithm (a symplectic method) to investigate the number dependence of the three transport coefficients being investigated here. Our results for the thermal conductivity study concentrate on the symplectic methods, pV2, vV2 and MA2 and Table 4 summarizes our results for these three methods at five different time-steps. These results support the findings from the previous sections on the shear viscosity and diffusion studies: for essentially large time-step size $\Delta t^* = 0.02$ all three symplectic algorithms approximate the thermal conductivity quite well yet with larger error bars than those found at the smaller time-step size $\Delta t^* \leq 0.015$.

5. Summary and conclusions

In this study, the results of using symplectic integrators for transport property simulations were presented and compared those obtained with nonsymplectic integrators. The SI results are superior to those obtained with nonSI integrators, G4 and RK4, especially for large time-steps. We found that the SIs provide excellent results for total and kinetic energy conservation which is a key to successful simulations with large time-steps. The uncertainties in the results obtained for the transport coefficients using symplectic integrators were: diffusion coefficients based on either the Green–Kubo or Einstein formalism 1%, shear viscosity 5–6%, and finally for thermal conductivity, approximately 10%. It is important to emphasize the successful large step size estimates for all three transport coefficients studied here. Essentially, the simulations carried out at $\Delta t^* = 0.02$ estimate the transport coefficients to within 2% (or less) of the corresponding value obtained in the $\Delta t^* = 0.0025$ simulations.

Acknowledgements

JR would like to acknowledge the Thai Government's Science and Technology support for a Ph.D. scholarship. DI would like to thank CEPR for its gracious hospitality and support at the CSM. This work was supported by the US Department of Energy, Grant 95ER-FG02-41568.

References

[1] D.A. McQuarrie, Statistical Mechanics, Harper, New York, 1976.
[2] W.G. Hoover, Nonequilibrium Molecular Dynamics, Springer, Berlin, 1986.
[3] W.G. Hoover, Computational Statistical Mechanics, Elsevier, Amsterdam, 1991.
[4] D.J. Evans, G.P. Morriss, Statistical Mechanics of Nonequilibrium Liquids, Academic Press, London, 1990.
[5] L. Verlet, Phys. Rev A 159 (1967) 98–103.
[6] L. Verlet, Phys. Rev. A 165 (1968) 201–214.
[7] L. Verlet, Phys. Rev. A 2 (1970) 2514–2527.
[8] A. Rahman, Phys. Rev. 36 (1964) A405–A411.
[9] W.G. Hoover, A.J.C. Ladd, R.B.H., B.L. Holian, Phys. Rev. A 21 (1980) 1756–1760.
[10] C. Hoheisel, R. Vogelsang, Comp. Phys. Rep. 8 (1988) 1–70.
[11] D.J. Evans, G.P. Morriss, Comp. Phys. Rep. 1 (1984) 299–343.
[12] M. Schoen, C. Hoheisel, Mol. Phys. 56 (1985) 653–672.
[13] D.M. Heyes, J. Chem. Soc., Faraday Trans. 2 79 (1983) 1741–1758.
[14] D.M. Heyes, J. Chem. Soc., Faraday Trans. 2 80 (1984) 1363–1394.
[15] D.M. Heyes, G.P. Morriss, D.J. Evans, J. Chem. Phys. 83 (1985) 4760–4766.
[16] J.J. Erpenbeck, Phys. Rev. A 38 (1988) 6255–6266.
[17] R.D. Ruth, IEEE Trans. Nucl. Sci. 30 (1983) 2669–2671.
[18] H. Yoshida, Phys. Lett. A 150 (1990) 262–268.
[19] H. Yoshida, Celest. Mech. Dynam. Astron. 56 (1993) 27–43.
[20] M.E. Tuckerman, B.J. Berne, G.J. Martyna, J. Chem. Phys. 94 (1991) 6811–6815.
[21] M. Tuckerman, B.J. Berne, G.J. Martyna, J. Chem. Phys. 97 (1992) 1990–2001.
[22] M. Tuckerman, B.J. Berne, G.J. Martyna, J. Chem. Phys. 99 (1993) 2278–2279.
[23] Z. Xu, J.J. de Pablo, S. Kim, J. Chem. Phys. 102 (1995) 5836–5844.
[24] M.J. Stevens, M. Mondello, G.S. Grest, S.T. Cui, H.D. Cochran, P.T. Cummings, J. Chem. Phys. 106 (1997) 7303–7314.
[25] M.E. Tuckerman, M. Parrinello, J. Chem. Phys. 101 (1994) 1302–1315.
[26] M.E. Tuckerman, M. Parrinello, J. Chem. Phys. 101 (1994) 1316–1329.
[27] J.M. Haile, Molecular Dynamics Simulations, Wiley, New York, 1992.
[28] R.I. McLachlan, P. Atela, Nonlinearity 5 (1992) 541–562.
[29] D. Levesque, L. Verlet, Phys. Rev. A 7 (1973) 1690–1700.
[30] D.M. Heyes, The Liquid State: Applications of Molecular Simulations, Wiley, New York, 1998.